Wireless Complex Permittivity Measurement Using Resonant Scatterers and a Radar Approach

Florian Requena, Nicolas Barbot, Darine Kaddour, Etienne Perret

Wireless Complex Permittivity Measurement Using Resonant Scatterers and a Radar Approach

Florian Requena, *Student Member, IEEE,* Nicolas Barbot, *Member, IEEE,*
Darine Kaddour, *Member, IEEE,* and Etienne Perret, *Senior Member, IEEE*

***Abstract*—In this paper, a method to characterize complex permittivity of dielectric is presented. The back-scattered signal from a resonant scatterer placed in contact with the dielectric is used to estimate the dielectric properties. The proposed method was tested in simulation and validated in practice using different dielectric samples and different dielectric thicknesses. This method is wireless, non-destructive, with no restriction on the sample thickness and is done using a VNA and an antenna. Discussions on the geometry of the resonator as well as the calibration step is proposed in order to improve the sensing capability of the approach. Monte-Carlo simulation has been performed to define a confidence interval for the values extracted with the proposed approach in the range 1 to 3.5 for permittivity and 0 to 0.2 for $\tan\delta$ with a SNR of 20dB. For example, a permittivity $\varepsilon_r = 3.54 \pm 0.06$ and $\tan\delta = 0.0024 \pm 0.003$ has been measured for Rogers RO4003C and $\varepsilon_r = 2.31 \pm 0.05$ and $\tan\delta = 0.004 \pm 0.002$ for Duroid RT5880 with different thicknesses. It is also shown in simulation that the approach is compatible with materials having loss tangents up to 0.5, and real permittivity up to 10.**

***Index Terms*—Complex permittivity, Radar, Resonant, Scatterer, Wireless measurement**

I. Introduction

MICROWAVE sensors interest has increased over the last decades. Various sensors able to measure quantities such as temperature [1], humidity [2], gas [3], strain [4] without batteries or electronic chips have been published. This wireless approch based on radio-frequency (RF) waves caught the curiosity for sensor applications due to its low-profile (often planar and single layer sensors), its accuracy, its price and finally its infinite life-time of operation due the to absence of electronic parts. The RF waves also provide advantages such as wireless measurements that allow the reading of multiple sensors at the same time, in realtime, even with obstacles [5]. Such RF approaches have also been developed to do metrology. We can cite for example the characterization of the materials thermal dilatation [6] or the complex permittivity [7].

Concerning the complex permittivity measurements, numerous works can be found in the litterature [8], [7], [9], [10]. These methods can be divided in two main categories : resonant and non-resonant approaches. In non-resonant approaches, coaxial measurements are commonly used and standardized [11]. The coaxial method consists in measuring the transmission and reflection coefficients of a coaxial transmission line filled with the dielectric under-test [12], [13]. The transmission/reflection principle is also transposed to other techniques such as waveguides [14] or free-space measurements [15]. These techniques are simple to implement, work on wide frequency band but the major drawback is their low accuracy, especially on the losses extraction for low-loss dielectrics. On the other hand, resonant methods allow to have higher accuracies and to measure lower losses but are restricted in the frequency response. Cavity measurements [16], [17] are widely used for dielectric characterization. Besides, various resonator topologies have been published in the litterature. We can cite, open resonator [18], [19] and dielectric rod resonators short circuited at both ends by two parallel conducting plates [20], [21]. For the solid dielectric materials which are exclusively dealt with in this paper, a major problem is the accurate machining of a specimen of the material to fit closely into the resonator or waveguide.

In the recent years, planar microstrip resonators using the under-characterization material as a substrate were introduced in [22], [23], [24]. This technique allows a wireless measurement based on a radar principle and allows to avoid the machining drawback. While in [22], the RF access lines conventionally used to connect to a VNA [8] were replaced by antennas, [24] and [23] present an approach where only a resonant target is present without any antenna. In [23], the resonant target (open metal ring on a known dielectric substrate) is realized on PCB. Here, the material to be characterized is a small dielectric slab of a few mm length, positioned in the opening of the ring. This method offers the advantages of being easy to implement and low-cost like wireless test-benches (only one antenna and a VNA are needed). In addition, it offers advantages (real-time and accurate measurements) making it a potential solution for dielectric characterization. Contrary to [20], [21] the sample under test does not need to be precisely positioned in the test bench (e.g. the distance between the antenna and the resonator can be changed easily). In these works, the permittivity [24], or the complex permittivity [22], [23] is directly linked to the resonance impacting both its frequency and its attenuation. However in [22], [23], measurements or simulations are used to fit a model which describes the resonance frequency behavior.

In this paper, the complex permittivity is related to the resonance with a theoretical approach and an analytical formula

Manuscript received X; revised X; accepted X. Date of publication X; date of current version X. This project has received funding from the European Research Council (ERC) under the European Union's Horizon 2020 research and innovation program (grant agreement No 772539). This work is also supported by Univ. Grenoble Alpes. (*Corresponding author: Requena Florian.*). The authors are with Univ. Grenoble Alpes, Grenoble INP, LCIS, F-26000 Valence, France. E. Perret is also with Institut Universitaire de France, Paris, France.

is obtained. In addition, the characterization frequency band, can be increased by using different resonators operating at different frequencies. As in [24], the approach is based on the use of an independent metallic resonator which is attached to the dielectric plate to be measured and whose thickness is assumed to be known. However, here a more general approach is introduced in order to determine the dielectric losses. Compared to [23], the sensitivity is maximized by using no other dielectric than the one to characterize. Besides, there is no need to machine the dielectric : its dimensions should largely cover the metallic resonator.

In Section II the equations relating the resonance to the complex permittivity will be introduced. Section III focuses on the complex permittivity extraction from radar measurements. Section IV and V present simulations and measurements of several samples as well as discussions on the accuracy and sensitivity of the proposed approach. Finally, Section VI will conclude the paper.

II. Complex Resonance Frequency

The principle of the measurement is illustrated in Fig. 1a, which shows the measurement method based on the acquisition of a backscattered signal from a resonator in contact with the dielectric to be characterised. In this study the loop resonator shown in Fig. 1b will be used.

Using the Singularity Expansion Method (SEM), it can be shown that in the time domain, the signal back-scattered $u(t)$ by a resonator can be written as an exponentionally damped sinusoidal as follows :

$$u(t) = Ae^{-\sigma(t-2\tau)}\cos(\omega(t-2\tau))\Gamma(t-2\tau) \tag{1}$$

where A is the amplitude of the back-scattered signal, Γ is the Heavyside function and τ the propagation constant. This signal is illustrated Fig. 2. Let define the complex resonance frequency $s = \sigma + j\omega$ to analyze the radar response of a resonant target in terms of damping factor σ and angular resonant frequency ω. The back-scattered signal can be re-written as :

$$u(t) = A \times \text{Re}\left[e^{-s(t-2\tau)}\right] \times \Gamma(t-2\tau), \tag{2}$$

where Re defines the real part. If a simple loop resonator is used (as illustrated in Fig.1) for our radar target, its resonance frequency f_r is defined by [25]:

$$f_r = \frac{c}{2L\sqrt{1+\frac{\varepsilon_r-1}{2}q}}, \tag{3}$$

where c is the speed of light in vacuum, L the length of the resonant scatterer, q the filling factor which is a coefficient to take into account the support thickness [26] and ε_r the permittivity of the dielectric under-test. For this reason, the resonance frequency of a resonator placed on a lossless dielectric is associated to the variable s_r by :

$$s_r = \sigma_r + j\omega_r = \sigma_r + j2\pi\frac{c}{2L\sqrt{1+\frac{\varepsilon_r-1}{2}q}}. \tag{4}$$

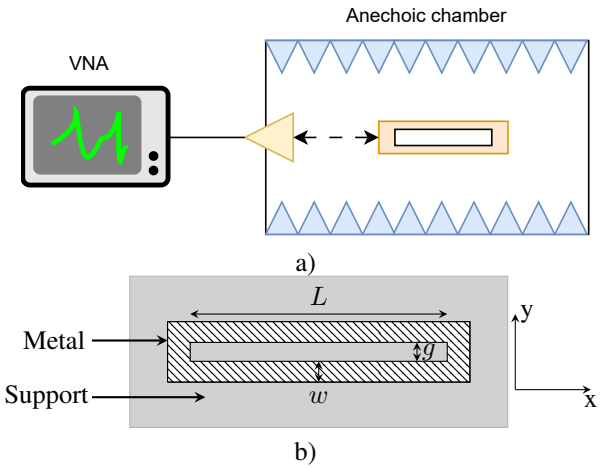

Fig. 1. a) Principle of the measurement of the scatterer. b) Loop resonator considered in this study. The support is the dielectric under-test defined by $\varepsilon = \varepsilon_r(1 - j\tan\delta)$.

Even in the lossless case σ_r is linked to metallic losses and radiation losses so it is not zero. When a dielectric presents RF losses, its permittivity can be written as $\varepsilon = \varepsilon_r(1 - j\tan\delta)$, where $\tan\delta$ is the dielectric loss tangeant, hence the complex resonance frequency can be introduced :

$$f_d = \frac{c}{2L\sqrt{1+\frac{\varepsilon_r(1-j\tan\delta)-1}{2}q}}, \tag{5}$$

which gives the expression of the complex resonance frequency in the case of electrical loss s_d :

$$s_d = \sigma_r + jBe^{-\frac{j}{2}\tan\left(\frac{\tan\delta q\varepsilon_r}{2+q(\varepsilon_r-1)}\right)}, \tag{6}$$

where $B = \dfrac{\omega_0}{\sqrt{1+\frac{\varepsilon_r-1}{2}q}\left(1+\left(\frac{\tan\delta q\varepsilon_r}{2+q(\varepsilon_r-1)}\right)^2\right)^{1/4}}$.

Note that the subscript d is used hereafter to designate expressions where the losses of the dielectric to be characterized are taken into account. For low losses, ($\tan\delta \ll 1$) which is usually the case for RF substrates, the complex resonance frequency f_d can be written :

$$f_d \simeq F_0\left(1 - \frac{j}{2}X - \frac{3}{8}X^2\right), \tag{7}$$

where $F_0 = \dfrac{c}{2L\sqrt{1+\frac{\varepsilon_r-1}{2}q}} = \dfrac{f_0}{\sqrt{1+\frac{\varepsilon_r-1}{2}q}}$ and $X = \dfrac{\tan\delta q\varepsilon_r}{2+q(\varepsilon_r-1)}$. Therefore, the variable s_d at the complex resonance frequency f_d is now given by :

$$s_d = \sigma_d + j\omega_d = \left(\sigma_0 + \frac{1}{2}W_0X\right) + jW_0\left(1 - \frac{3}{8}X^2\right), \tag{8}$$

where $W_0 = 2\pi F_0$. After identification, the damping factor and frequency at resonance for a lossy dielectric (σ_d, ω_d) can be expressed by :

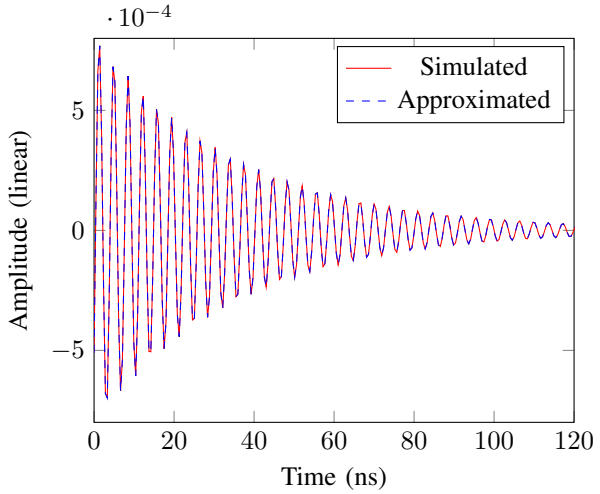

Fig. 2. Time domain back-scattered signal from a loop resonator in simulation.

$$\begin{cases} \sigma_d = \sigma_0 + \dfrac{\omega_0}{2\sqrt{1+\dfrac{\varepsilon_r-1}{2}q}} \dfrac{\tan\delta q\varepsilon_r}{2+q(\varepsilon_r-1)} & \text{(9a)} \\ \omega_d = \dfrac{w_0}{\sqrt{1+\dfrac{\varepsilon_r-1}{2}q}} \left(1-\dfrac{3}{8}\left(\dfrac{\tan\delta q\varepsilon_r}{2+q(\varepsilon_r-1)}\right)^2\right) & \text{(9b)} \end{cases}$$

.

Note that in (9b) only ε_r and $\tan\delta$ are unknown. Indeed, (σ_0, ω_0) and (σ_d, ω_d) are the damping factor and the resonance frequency measured for a loop resonator with no support and with the dielectric under-test respectively. Note that the length L does not affect the measurement. Also, different lengths can be used to charaterize the losses at different resonance frequencies. The coefficient q can be directly calculated using [26] or obtained through simulations as explained later in Section IV. It is possible from the measurement of the back-scattered signal of a resonator (see Fig. 2) to extract the values of damping factors and resonance frequencies. Several techniques allow the extraction of these coefficients from the backscattered electromagnetic signature of a resonant scatterer. Approaches applied to the time domain representation of the signal [27] or to a frequency domain representation [28] are both considered in the litterature. Fig. 2 presents an example of time domain back-scattered signal (in simulation) obtained from the loop illustrated in Fig. 1. In this figure we can see both the backscattered signal obtained by simulation and the signal reconstructed from the extraction of the damping factors and the resonance frequencies based on [27].

For a rectangular loop of this type, there is a trade-off between the RCS level and the quality factor value. This trade-off is primarily related to the width of the gap g between the two larger arms of the rectangular loop. The smaller the gap, the higher the quality factor and the lower the RCS. An optimisation on CST allowed to obtain a good compromise where the objective remains however to have a quality factor above 100 in air.

III. Permittivity Extraction

Equation (9b) can be re-written as :

$$\begin{cases} \tan\delta = 2(\sigma_d-\sigma_0)\dfrac{\sqrt{1+\dfrac{\varepsilon_r-1}{2}q}}{\omega_0}\dfrac{2+q(\varepsilon_r-1)}{q\varepsilon_r} \\ \overline{\omega}\sqrt{1+\dfrac{\varepsilon_r-1}{2}q} = 1-\dfrac{3}{2}\overline{\sigma}^2\left(1+\dfrac{\varepsilon_r-1}{2}q\right) \end{cases}, \tag{10}$$

where $\overline{\omega} = \dfrac{\omega_d}{\omega_0}$ and $\overline{\sigma} = \dfrac{\sigma_d-\sigma_0}{\omega_0}$. By letting $Y = \sqrt{1+\dfrac{\varepsilon_r-1}{2}q}$, the second equation can be expressed as a quadratic equation aY^2+bY+c with :

$$\begin{cases} a = \dfrac{3}{2}\overline{\sigma}^2 \\ b = \overline{\omega} \\ c = -1 \end{cases}. \tag{11}$$

The real positive solution Y is :

$$Y = \frac{-\overline{\omega}+\sqrt{\overline{\omega}^2+6\overline{\sigma}^2}}{3\overline{\sigma}^2}. \tag{12}$$

Then the real part of the permittivity ε_r can be found using (12) with :

$$\begin{aligned} \varepsilon_r &= 1+2\frac{Y^2-1}{q} \\ &= 1+\frac{2}{q}\left(\left(\frac{-\overline{\omega}+\sqrt{\overline{\omega}^2+6\overline{\sigma}^2}}{3\overline{\sigma}^2}\right)^2-1\right) \end{aligned} \tag{13}$$

and the losses can be found using (9b) and (13) with :

$$\tan\delta = 4\overline{\sigma}\frac{\left(\dfrac{-\overline{\omega}+\sqrt{\overline{\omega}^2+6\overline{\sigma}^2}}{3\overline{\sigma}^2}\right)^{5/2}}{q+2\left(\dfrac{-\overline{\omega}+\sqrt{\overline{\omega}^2+6\overline{\sigma}^2}}{3\overline{\sigma}^2}-1\right)^2}. \tag{14}$$

These formulas are used to extract ε_r and $\tan\delta$. The dielectric characterization requires 2 measurements for the loop resonator : the first with no support and the second with the dielectric under test.

IV. Simulations

Simulations have been carried out using CST MW to validate the introduced equations. A farfield E-probe with the Time domain solver is used. The loop resonator configuration of Fig. 1 has been used. As previously explained, for a rectangular loop of this type, there is a trade-off between the RCS level and the quality factor value. An optimisation on CST allowed to obtain a good compromise. Fianl dimensions are $L = 50$mm, $w = 1.4$mm and $g = 2$mm. The metal is 1mm thick. The loop is placed on the dielectric material to be characterized with permittivity ε_r and loss tangent $\tan\delta$. The dielectric height is 1mm so $q \simeq 0.58$ based on [26]. The excitation is a plane wave polarized along the $\vec{y}$-axis (see Fig.

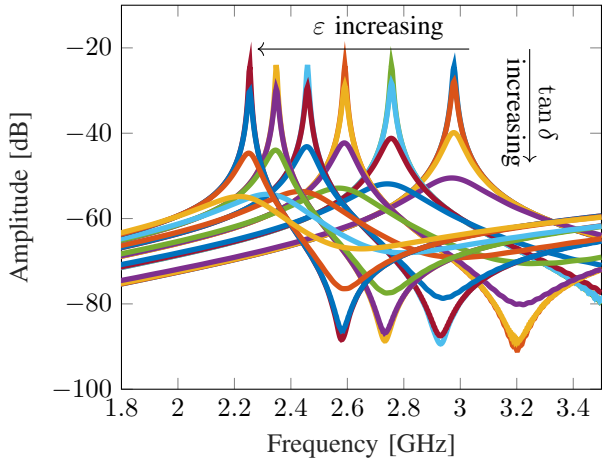

Fig. 3. Simulated back-scattered E-field in amplitude for $\varepsilon_r = [1 : 0.5 : 3.5]$ and $\tan\delta \in [0, 0.005, 0.05, 0.2]$ for the loop resonator of Fig. 1 impringed by a plan wave. Dielectric height is 1mm.

1b). The probe used to obtain the backscattered signal is placed 1 meter away from the resonator. The simulated back-scattered E-fields for different values of ε_r and $\tan\delta$ are plotted in Fig. 3. These simulations show the impact of the variation of the dielectric parameters on both the resonance frequency and the damping factor.

Based on these simulations, the Matrix Pencil method [27] is used to extract the complex natural resonance (CNR) $s = \sigma + j\omega$. For each configuration the resonance frequency $f = \omega/2\pi$ as well as the damping factor σ are plotted in Fig. 4. The correspondence betewen the values of the complex permitivity and the number (noted "Run ID") associated to the simulation is given in Table. I. We can see that resonance frequency decreases with an increase of the real and also of the imaginary part of the permittivity. The damping factor mostly increases with the imaginary part of the permittivity (losses). Fig. 4 also presents results obtained with (9b) which show a good agreement with the simulations.

The study of the error obtained from (9b) will be realized in the measurement section. Indeed in simulation, even if the structure is relatively simple, the error will be directly linked to the models used in the EM simulator to take into account the losses, which is not what we seek to study in this article.

Based on the values of the simulated frequency resonance and damping factor, the complex permittivity can be extracted using (13) and (14). Estimated ε_r and $\tan\delta$ are plotted in Fig. 5. Again, we can notice that the extracted values are in good agreement with the simulated ones.

A discussion will be made concerning the sensitivity and accuracy of the proposed method based on the resonant scatterer. As shown in (9b), the only factor that impacts the results is the coefficient q. Indeed, the higher the value of q, the larger the shifts in the signal amplitude or on the resonance frequency. Thus better sensibility on the complex permittivity extraction can be expected. To increase q, the loop geometry as well as the dielectric under-test thickness should be considered when designing the resonator [26]. A simulation with two different gap values for the loop is presented in Fig. 6. We can see that a

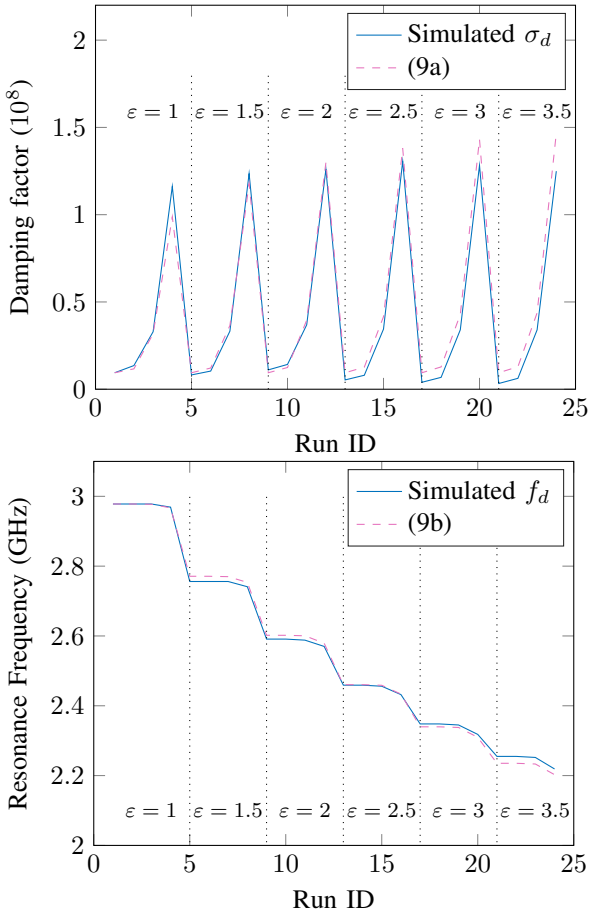

Fig. 4. Comparision between simulations and equations : a) Damping factor b) resonance frequency.

smaller gap induces a higher value for q and so higher shifts in the resonance frequency is observed. The study of the variation of the resonance frequency as a function of q, more exactly the computation of $d(\omega_r/\omega_0)/dq$ by derivating (9b) [see Fig. 8] allows to show analytically that the resonance frequency of the resonator on the dielectric varies the more when the value of q is high. This explains why the error obtained is smaller for thick substrate where q is large in this case. Similarly, the greater the thickness of the substrate, the lower the resonance frequency and therefore the greater the frequency variation compared to the case without the dielectric. Measuring this larger offset leads to less error. Futhermore, Fig. 7 presents the simulated filling factor q for different dielectric heights and different resonator metal thicknesses. We should notice that [26, eq. (21)] offers a good agreement with simulations for very thin metal (the metal thickness is considered infinitely thin). When the resonator's metal is thicker, [26, eq. (21)] is no more valid to determine q with accuracy. For this reason, extracted values of q obtained from simulations and shown in Fig. 7 will be used in the section V for dielectric characterization. Contrary to the classical cavity method, this approach does not require thin dielectric sample to work. Indeed, as shown in Fig.7, the thicker the dielectric, the larger the value of q, which improves the final estimation of the complex permittivity.

TABLE I
CORRESPONDENCE BETWEEN SIMULATIONS "RUN ID" AND $(\varepsilon_r, \tan\delta)$.

Run ID	1	2	3	4	5	6	7	8	9	10	11	12	13	14	15	16	17	18	19	20	21	22	23	24
ε_r	1	1	1	1	1.5	1.5	1.5	1.5	2	2	2	2	2.5	2.5	2.5	2.5	3	3	3	3	3.5	3.5	3.5	3.5
$\tan\delta$	0	0.005	0.05	0.2	0	0.005	0.05	0.2	0	0.005	0.05	0.2	0	0.005	0.05	0.2	0	0.005	0.05	0.2	0	0.005	0.05	0.2

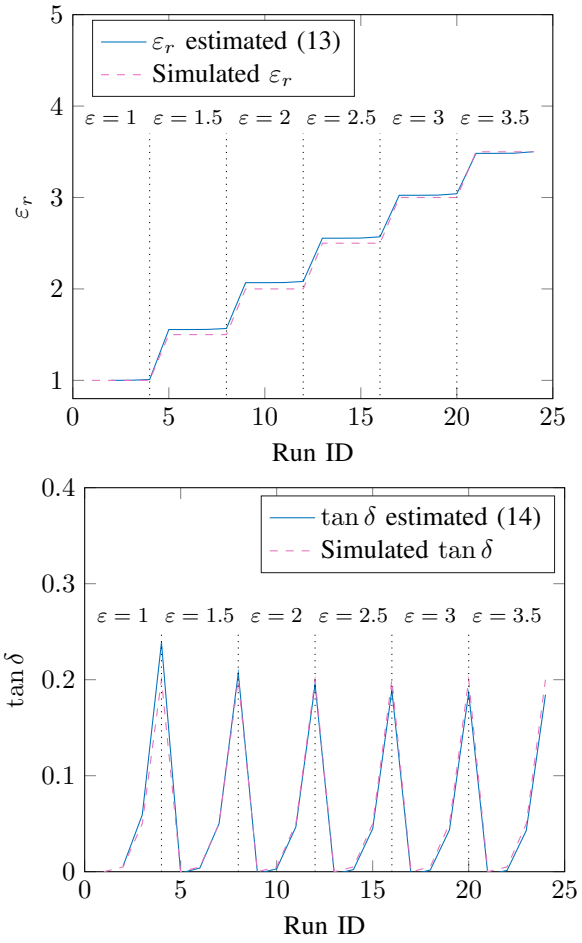

Fig. 5. ε_r and $\tan\delta$ estimated with (13) and (14) respectively. The different values used for the study and corresponding to a ID number are shown in Table I.

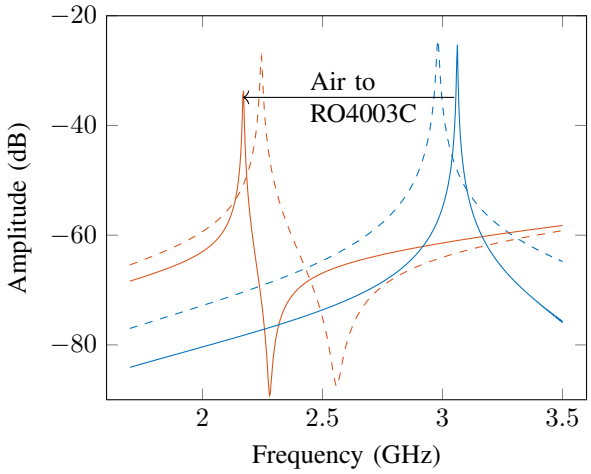

Fig. 6. Influence of the gap g of the loop on the extraction of the complex permittivity: gap $g = 0.5$mm ($q = 0.77$) [plain line] and $g = 2$mm ($q = 0.6$) [dashed line]. The blue curves correspond to a permittivity of $\varepsilon = 1$ and the red ones to a permittivity of $\varepsilon = 3.55 * (1 - \mathrm{j}0.0021)$.

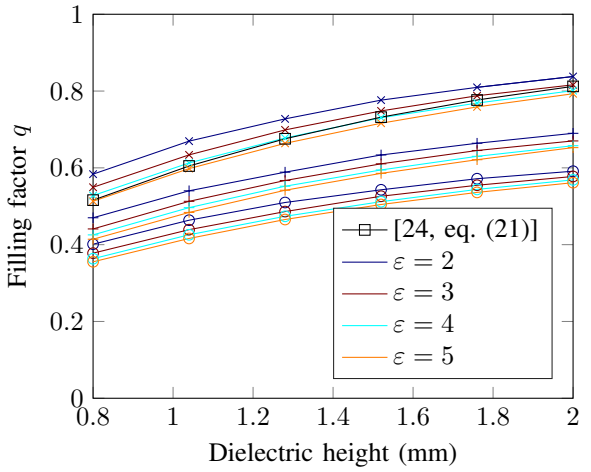

Fig. 7. Filling factor q as a function of the dielectric height and the metal thickness. $\times$ markers correspond to a metal thickness of 0.01mm, + markers to a thickness of 0.5mm and ◯ markers to 1mm. □ is the q calculated using [26, eq. (21)].

V. MEASUREMENTS

The proposed approach will be validated by measurements using different samples. The different samples and dielectric thicknesses evaluated in practice are given in Table. II. The "Red" test sample was characterized using the cavity method for complex permittivity measurements (the Damaskos, Inc. Model 08 Thin Sheet Tester that measures the dielectric properties of low loss materials over the approximate band of 800-4000 MHz in a non-destructive manner).

The following protocol was used for the measurements : firstly, the loop resonator is measured in the air using a mono-static configuration inside an anechoic chamber (see Fig. 1 and Fig. 9). The VNA 5222A by Agilent was used. The source power of VNA is equal to 0 dBm. The frequency sweep ranging from 2 to 3 GHz with 4001 points is considered. A mono-static configuration with Satimo (QH800) quad ridged open boundary antennas (0.8–12 GHz) is used. We have used a dual linear antenna for this measurement, however any simpler (linear polarization) and less expensive (e.g. a Vivaldi antenna realized on PCB) would achieve the same performance for this application. Indeed, to keep the same SNR, with a less directive antenna, it is sufficient to decrease the antenna-resonator distance. Compared to [24] where a bi-static configuration was used for the measurement, the results presented here were obtained with a mono-static configuration, which is simpler to implement and for which it is shown to be

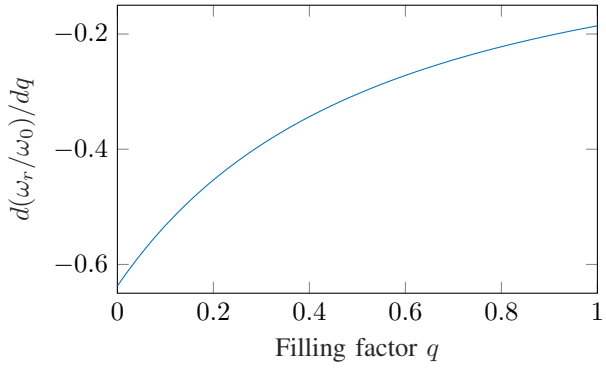

Fig. 8. The study of the variation of the resonance angular frequency ω as a function of the filling factor q.

sufficient to achieve the required degree of accuracy for the introduced extraction. The loop resonators were obtained by cutting a 0.5mm thick metal plate with a laser. Dimensions are L = 50.82mm, w = 1.43mm and g = 2.07mm. In the case, high purity copper metal has been chosen for the fabrication (more than 99% purity) [29].

Tape was used to suspend the loop in the air (see Fig. 9a) to be as close as possible to a free-space condition. The tape was also used to attach the loop to the samples as can be seen in Fig. 9b. Indeed, the use of tape for measurement is very significant in minimising the gap between the dielectric and the loop. This is especially true since these two elements are never perfectly planar (especially the metallic loop) and therefore the tape helps to keep them in touch during the measurement. The way in which the tape was used to clamp the loop was studied both in simulation and in practice to have as little impact as possible on the backscattered signal. The configuration chosen is shown in Fig. 9a and provides the best compromise between a very low impact on the resonant frequency, damping factor and a very good maintenance of the loop on the dielectric. It is however important to note that to consider as much as possible the presence of the tape in the method, we used tape both for the measurement in air (Fig. 9a) and when the loop is placed on the dielectric. This is a way to reduce the effect of tape in the measurement method introduced.

Matrix Pencil Method [27] is used on the S-parameters to evaluate (σ_0, ω_0). Secondly, the loop resonator was taped to the sample under-test as illustrated in Fig. 9b. Matrix Pencil is used once again on the S-parameters to evaluate (σ_r, ω_r). Finally, (13) and (14) are used to estimate the complex permittivity of the sample. The value of q is obtained based on the results presented in Fig. 7 for the corresponding dielectric thickness and for the 0.5mm metal thickness resonator used in practice. An example of measured S-parameters is given in Fig. 10 for different substrates. For each of them, the extracted dielectric parameters are given in Table II. We can see that the estimated complex permittivity is close to the provider's informations for the different samples and different dielectric thicknesses. There is only a difference in the losses of the Duroid RT5880. Indeed, the measured losses for the Duroid RT5880 (both heights) using the proposed approach grant losses 4 times larger at 2.5GHz than the ones given by the provider at 10GHz. Although some of the difference may be attributable to the difference in frequencies, it is also possible that the limitations of the approach to the minimum loss tangents that can be measured can be observed here. We were also interested in evaluating the maximum loss tangent values that the method can extract. Indeed, this method relies on the extraction of the resonance frequency and the damping factor, and this extraction will be impacted by a too high loss tangent value. In simulation we have observed with the loop used that it becomes difficult to characterise dielectrics with loss tangents greater than 0.4. This shows that in order to reach higher values, it is necessary to work on the design of the loop resonator, or even to opt for another resonator.

It is also important to notice that these values are frequency dependent (especially $\tan\delta$ in this frequency band). The proposed method allows to measure the complex permittivity at the resonance frequency of the scatterer when it is placed on the sample to characterize. For this reason, designing different resonator lengths is a solution to determine the complex permittivity at multiple frequencies. Scatterers used in the paper were designed to have their fundamental resonance frequency close to 3GHz in the air.

Now that the approach is validated in practice, a second approach is presented in order to correct systematic errors. When the resonator is taped to the dielectric, a small air gap could always be present in between the resonator and the dielectric changing the effective permittivity seen by the resonator. Also, tape induced a constant frequency shift due to its presence. When resonators are taped several times to the same dielectric, we notice that the resonance frequency does not vary a lot meaning that the air gap (with tape) is constant between measurements. The improvement proposed here is to use a known dielectric for calibration to estimate the "in-air" resonator values. Then the estimated "in-air" values are used to characterize a second dielectric under-test. For a known dielectric and so its $(\varepsilon_{cal}, \tan\delta_{cal})$, we can write :

$$\begin{cases} \omega_0 = \dfrac{w_{cal}\sqrt{1+\dfrac{\varepsilon_{cal}-1}{2}q}}{\left(1-\dfrac{3}{8}\left(\dfrac{\tan\delta_{cal}q\varepsilon_{cal}}{2+q(\varepsilon_{cal}-1)}\right)^2\right)} \\ \sigma_0 = \sigma_{cal} + \dfrac{\omega_0}{2\sqrt{1+\dfrac{\varepsilon_{cal}-1}{2}q}}\dfrac{\tan\delta_{cal}q\varepsilon_{cal}}{2+q(\varepsilon_{cal}-1)} \end{cases} . \quad (15)$$

For this reason, the initial measurement in air can be replaced by a measurement on a known dielectric and (15) can be used to determine $(\sigma_0, \tan\delta_0)$. By using this procedure to estimate the RT5880 using the RO4003C (both with a thickness of around 0.8mm) as a calibration dielectric permits to measure $\varepsilon_{RT} = 2.32$ and $\tan\delta_{RT} = 0.003$ at 2.6GHz hence improving a little the results.

Note that in such a case the two dielectrics don't need to have the same thickness. Indeed, the value corresponding to the measurement of the loop and the dielectric of reference is computed using (15) with the filling factor q corresponding to this dielectric and so its thickness. Then the permittivity

a)

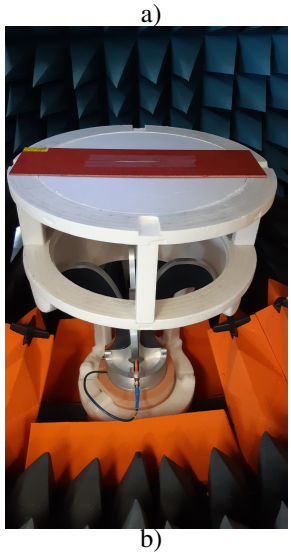

b)

Fig. 9. Testbench used for the measurement. a) Initial measurement to evaluate (σ_0, ω_0). b) Measurement of the "Red" test sample where the loop has been positioned over of the sample with tape.

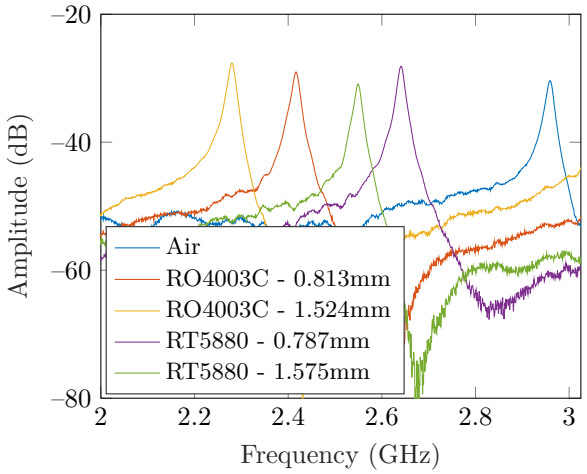

Fig. 10. Measurement of the S_{11} parameters for a loop resonator in air (blue) and on the different substrates.

is estimated with (13) and (14) with the filling factor of the dielectric under-test.

VI. Discussions

The resonance frequency and damping factor are related to the geometry and materials constituting the resonator. Indeed, from a theoretical point of view, and this is also what makes this method so interesting, the quantities involved in the extraction (resonance frequency and quality factor) are aspect-independent parameters [28], which means that they are not linked to the measurement bench (such as the gain of the antennas, the distance, the orientation of the antennas...). It is therefore possible to carry out measurements at two different distances (measurement without and with dielectric), but this is of very limited interest in practice. Note that this measurement can easily be implemented in controlled environment for metrology measurements. In this respect, the maximum distance that can be used with this technique will depend on the environment and the measurement time (linked in particular to the averaging used) and the precision of the measurement equipment. However, a notable limitation of the approach occurs at the level of dielectrics with significant losses. Indeed, we could see in simulation (not shown in the paper) that for loss tangent higher than 0.5, it is no longer possible to extract the quality factor. This means that it is no longer possible to access the material losses. As far as the range of values on the real part of the permittivity is concerned, we did not observe such limitations. Indeed, we were able to test that a material with a permittivity of 10 was perfectly compatible with the introduced approach.

In practice, if the distance between the resonator and the antenna increases, the SNR will decrease, so the estimation of the poles and then the complex permittivity will be impacted. Monte-Carlo (MC) simulation for a SNR of 20dB on the S-parameters is shown in Fig. 11. Noise was added on the time response signal of the simulated loop on a lossy dielectric substrate. The simulated permittivity and losses range respectively from 1 to 3.5 and 0 to 0.1. This simulates the effect on complex permittivity extraction when the distance between the antenna and the resonator is increased. We can see in these numerical simulations shown in Fig. 11 the impacts in terms of errors and uncertainties on the extracted permittivity.

We can see that a SNR of 20dB does not introduce errors or uncertainties sufficient to modify the extraction. However, as expected, it will introduce slight uncertainties on the loss tangent. By lowering the SNR to 5dB, similar results were obtained on the extracted permittivity. The measurement of the SNR in practice and the use of the presented MC simulation can allow the user to estimate the uncertainties on his measurement setup (noise, distance for antenna-resonator,...).

Sensing is improved when the estimation is robust to the noise, which is illustrated by the MC simulations presented Fig. 11. Sensing is also improved with higher variations of the measurand (higher variation usually means peaks easier to measure but also less correlated to noise). These variations of the resonance frequency in term of sensibility can be compared to others works [9]. Note that the present manuscript does not try to improve the sensitivity S [30, eq. (3)] but is rather on the theory and setup used to measure the complex permittivity. However, in Fig. 6, a simulation is made to illustrate how the

TABLE II
COMPARISON OF THE COMPLEX PERMITTIVITY OF THE SAMPLE GIVEN BY THEIR PROVIDER AND MEASURED BY THIS APPROACH

	Thickness (mm)	ε_r (provider)	$\tan\delta$ (provider)	ε_r (cavity method)	$\tan\delta$ (cavity method)	ε_r (this approach)	$\tan\delta$ (this approach)	Sensitivity S (this approach)
Rogers	0.813	3.55	0.0021 @2.5GHz	3.72	0.0029 @2.5GHz	3.54	0.0024 @2.4GHz	5.15%
RO4003C	1.524	3.55	0.0021 @2.5GHz	3.49	0.0014 @3GHz	3.59	0.0031 @2.2GHz	6.45%
Duroid	0.787	2.33	0.0012@10GHz	2.29	0.0018 @2.5GHz	2.31	0.004 @2.6GHz	4.61%
RT5880	1.575	2.33	0.0012@10GHz	2.29	0.0018 @2.5GHz	2.31	0.004 @2.5GHz	5.94%
Red	1.958	4.24	0.0173 @3.1GHz	4.25	0.018 @3.1GHz	4.27	0.012 @2.2GHz	10.71%

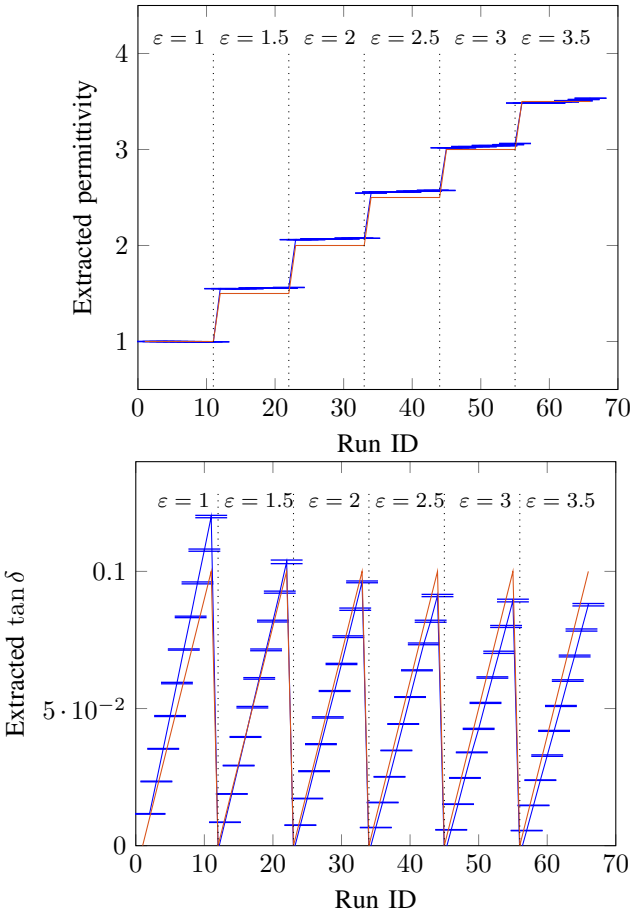

Fig. 11. Simulated complex permittivity in red and extracted complex permittivity in blue with a MC simulation with a SNR of 20dB. The simulated permittivity and losses range respectively from 1 to 3.5 and 0 to 0.1.

design of the loop can be improve to obtain higher values of S. In this simulation and for a gap g=0.5mm (plain line), a value of $S = \dfrac{(f_1 - f_2)}{f_1 \Delta\varepsilon} = 8.19\%$ is obtained. We can see that this design introduced a sensitivity 2.5 times higher than the most sensitive permittivity sensor presented in [9]. Note also that, the present work allows in addition to measure the losses of the dielectric which is not done in [9]. Sensitivities S obtained in measurements are given in Table II. A comparison of sensitivities S of different works is given in Table III. Table II also illustrates the impact of the resonator geometry already discussed in Section IV. Indeed, we can see that considering one dielectric, the sensitivity S increases with the thickness of the sample under-test as q increases.

Lastly, in [1], section X, it was shown that different resonator topologies can be used to improve even more this sensibility. The dipole over a ground plane shown in [1] can be used to obtain even higher sensitivity but it was not presented in the current paper since its utilization as a complex permittivity sensor seems more difficult to implement. The dipole resonator needs to be printed on the dielectric under test while the loop can be manually placed as it is done in the manuscript.

The MC simulation allows to define a confidence interval in the complex permittivity values extracted with the proposed approach. Indeed Fig. 12 presents the error between simulated values (entered in CST) and extracted values (with the introduced approach) for different simulated complex permittivity values. It is interesting to note that this error mainly characterises the accuracy of the model and indeed the values obtained here are very close to the deviation that could be calculated between the values entered on CST and extracted by the model presented in Fig. 5 (in this case no noise has been added contrary to the results in Fig. 11). Thus, further work on the model (for certain permittivity or loss ranges, for example through a calibration), could further improve the accuracy of the approach. It is also interesting to consider the uncertainties obtained through the MC simulation (see Fig. 11). Indeed, as can be seen in this figure, this uncertainty (for a confidence level of one standard deviation, i.e. approximately 68%) is very low compared to the errors shown in Fig. 12. This shows that the noise added in the MC simulation has very little effect on the value extracted by the approach, which shows a very good accuracy. Taking these elements into account, we can say that the real value (entered in CST) is located (in the worst-case scenario) in a confidence interval which can be estimated based on the errors plotted in Fig.12 and the uncertainty directly computed with the MC simulation. As the uncertainty is very small compared to the error, a confidence interval equal to +/- the error can be used here to give an idea of the accuracy that can be expected with this approach.

We note also that the results obtained in terms of measurement error are similar to those described in [31] where complex permittivity is sensed using a cavity method. Indeed, in [31], epoxy was characterized with a permittivity of 2.93 ± 0.11 and losses tangent of 0.028 ± 0.002. We can notice that the proposed approach allows to have similar results on the losses (also ± 0.002 in this work). The same applies to permittivity. The measurement results of the samples are collected in Table IV where the confidence interval has been added for each value

TABLE III
COMPARISON OF THE SENSITIVITY S OF DIFFERENT WORKS

	Frequency (GHz)	Sensitivity S
[32], [33]	7.6	2.6%
[34]	2.1	2.7%
[35]	4.5	2.2%
[9]	5.65	3.25%
This work	3	5.1% to 10.7%

TABLE IV
MEASURED SAMPLES AND CORRESPONDING CONFIDENCE INTERVAL COMPUTED BASED ON MC SIMULATION

	Thickness (mm)	ε_r (this approach)	$\tan\delta$ (this approach)
Rogers RO4003C	0.813 1.524	3.54 $\pm$0.06 3.59 $\pm$0.05	0.0024 $\pm$0.003 0.0031 $\pm$0.003
Duroid RT5880	0.787 1.575	2.31 $\pm$0.05 2.31 $\pm$0.06	0.004 $\pm$0.002 0.004 $\pm$0.002
Red	1.958	4.27 $\pm$0.03	0.012 $\pm$0.01

in order to give a more precise idea on the quality of the results obtained.

VII. CONCLUSION

In this paper, a method based on a radar approach to measure the materials' complex permittivity is introduced. A loop resonator is used to derivate the complex permittivity expression from back-scattered signals. Simulations and measurements have been realized to validate the proposed non destructive method on different dielectric slabs in the frequency band 2-3 GHz. Discussions on the resonator and dielectric geometries have been done in order to improve the accuracy of the extraction. Also, an additional calibration step using already known dielectric has been proposed and validated in practice to improve the estimations.

ACKNOWLEDGMENT

The authors are thankful towards Selim Azzouni for his help with cavity measurements and to Nathalie Franck for her help in proofreading the paper.

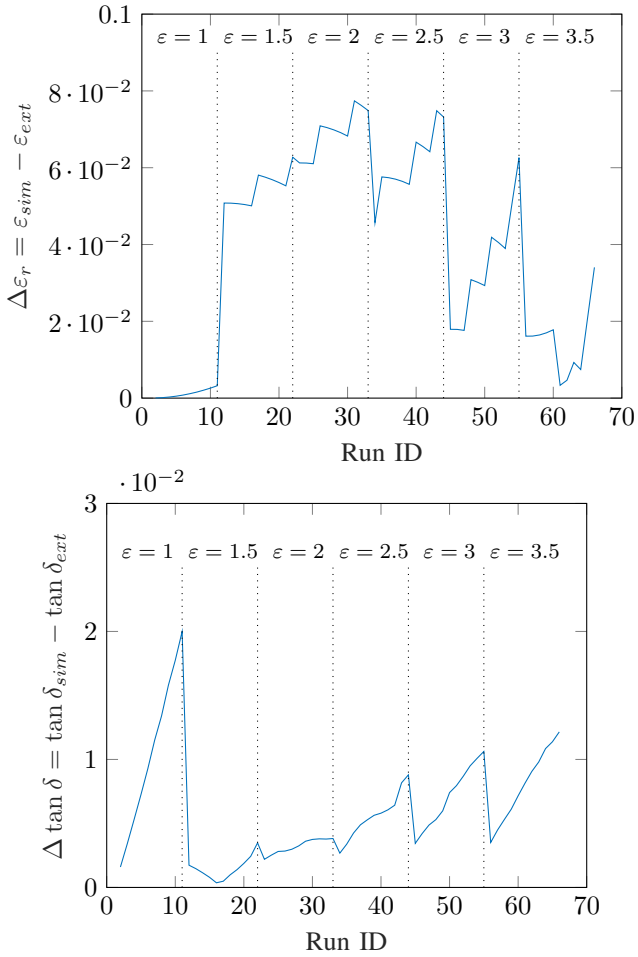

Fig. 12. Error for a) real part and b) losses between simulated values and extracted ones. The simulated permittivity and losses range respectively from 1 to 3.5 and 0 to 0.1.

REFERENCES

[1] F. Requena, M. Gilch, N. Barbot, D. Kaddour, R. Siragusa, F. Costa, S. Genovesi, and E. Perret, "Thermal modeling of resonant scatterers and reflectometry approach for remote temperature sensing," *IEEE Trans. Microw. Theory Tech.*, vol. 69, no. 11, pp. 4720–4734, 2021.

[2] Y. Feng, L. Xie, Q. Chen, and L.-R. Zheng, "Low-cost printed chipless rfid humidity sensor tag for intelligent packaging," *IEEE Sensors J.*, vol. 15, no. 6, pp. 3201–3208, 2014.

[3] L. Yang, R. Zhang, D. Staiculescu, C. Wong, and M. M. Tentzeris, "A novel conformal rfid-enabled module utilizing inkjet-printed antennas and carbon nanotubes for gas-detection applications," *IEEE Antennas Wireless Propag. Lett.*, vol. 8, pp. 653–656, 2009.

[4] T. T. Thai, H. Aubert, P. Pons, G. DeJean, M. M. Tentzeris, and R. Plana, "Novel design of a highly sensitive rf strain transducer for passive and remote sensing in two dimensions," *IEEE Trans. Microw. Theory Tech.*, vol. 61, no. 3, pp. 1385–1396, 2013.

[5] F. Requena, N. Barbot, D. Kaddour, and E. Perret, "Chipless RFID temperature and humidity sensing," in *2021 IEEE MTT-S International Microwave Symposium (IMS)*. IEEE, 2021, pp. 545–548.

[6] ——, "Contactless characterization of metals' thermal expansion coefficient by a free-space rf measurement," *IEEE Trans. Antennas Propag.*, vol. 69, no. 2, pp. 1230–1234, 2020.

[7] R. A. Alahnomi, Z. Zakaria, Z. M. Yussof, A. A. Althuwayb, A. Alhegazi, H. Alsariera, and N. A. Rahman, "Review of recent microwave planar resonator-based sensors: Techniques of complex permittivity extraction, applications, open challenges and future research directions," *Sensors*, vol. 21, no. 7, p. 2267, 2021.

[8] J. Krupka, "Frequency domain complex permittivity measurements at microwave frequencies," *Measurement Science and Technology*, vol. 17, no. 6, p. R55, 2006.

[9] S. Kiani, P. Rezaei, M. Navaei, and M. S. Abrishamian, "Microwave sensor for detection of solid material permittivity in single/multilayer samples with high quality factor," *IEEE Sensors J.*, vol. 18, no. 24, pp. 9971–9977, 2018.

[10] E. Massoni, G. Siciliano, M. Bozzi, and L. Perregrini, "Enhanced cavity sensor in SIW technology for material characterization," *IEEE Microw. Wireless Compon. Lett.*, vol. 28, no. 10, pp. 948–950, 2018.

[11] UTE, "Mesure de la permittivite et de la permeabilite de materiaux homogenes et isotropes a pertes dans le domaine des micro-ondes. methode de mesure en guide coaxial circulaire," *(Union Technique de l'Electricite et de la Communication)*, 1999.

[12] A. Nicolson and G. Ross, "Measurement of the intrinsic properties of materials by time-domain techniques," *IEEE Instrum. Meas. Mag.*, vol. 19, no. 4, pp. 377–382, 1970.

[13] J. Baker-Jarvis, E. J. Vanzura, and W. A. Kissick, "Improved technique for determining complex permittivity with the transmission/reflection method," *IEEE Trans. Microw. Theory Tech.*, vol. 38, no. 8, pp. 1096–1103, 1990.

[14] S. Bakhtiari, S. I. Ganchev, and R. Zoughi, "Open-ended rectangular

waveguide for nondestructive thickness measurement and variation detection of lossy dielectric slabs backed by a conducting plate," *IEEE Instrum. Meas. Mag.*, vol. 42, no. 1, pp. 19–24, 1993.

[15] F. I. Shimabukuro, S. Lazar, M. R. Chernick, and H. B. Dyson, "A quasi-optical method for measuring the complex permittivity of materials," *IEEE Trans. Microw. Theory Tech.*, vol. 32, no. 7, pp. 659–665, 1984.

[16] S. Li, C. Akyel, and R. G. Bosisio, "Precise calculations and measurements on the complex dielectric constant of lossy materials using tm/sub 010/cavity perturbation techniques," *IEEE Trans. Microw. Theory Tech.*, vol. 29, no. 10, pp. 1041–1048, 1981.

[17] S. Dmowski, J. Krupka, and A. Milewski, "Contactless measurement of silicon resistivity in cylindrical te01n mode cavities," *IEEE Instrum. Meas. Mag.*, vol. 29, no. 1, pp. 67–70, 1980.

[18] A. L. Cullen and P. Yu, "The accurate measurement of permittivity by means of an open resonator," *Proceedings of the Royal Society of London. A. Mathematical and Physical Sciences*, vol. 325, no. 1563, pp. 493–509, 1971.

[19] T. M. Hirvonen, P. Vainikainen, A. Lozowski, and A. V. Raisanen, "Measurement of dielectrics at 100 ghz with an open resonator connected to a network analyzer," *IEEE Instrum. Meas. Mag.*, vol. 45, no. 4, pp. 780–786, 1996.

[20] B. Hakki and P. D. Coleman, "A dielectric resonator method of measuring inductive capacities in the millimeter range," *IEEE Trans. Microw. Theory Tech.*, vol. 8, no. 4, pp. 402–410, 1960.

[21] Y. Kobayashi and M. Katoh, "Microwave measurement of dielectric properties of low-loss materials by the dielectric rod resonator method," *IEEE Trans. Microw. Theory Tech.*, vol. 33, no. 7, pp. 586–592, 1985.

[22] H. Lobato-Morales, A. Corona-Chávez, J. L. Olvera-Cervantes, R. A. Chávez-Pérez, and J. L. Medina-Monroy, "Wireless sensing of complex dielectric permittivity of liquids based on the RFID," *IEEE Trans. Microw. Theory Tech.*, vol. 62, no. 9, pp. 2160–2167, 2014.

[23] B. D. Wiltshire, T. Zarifi, and M. H. Zarifi, "Passive split ring resonator tag configuration for RFID-based wireless permittivity sensing," *IEEE Sensors J.*, vol. 20, no. 4, pp. 1904–1911, 2019.

[24] E. Perret, "Permittivity characterization based on radar cross measurements," in *2016 URSI International Symposium on Electromagnetic Theory (EMTS)*. IEEE, 2016, pp. 457–460.

[25] O. Rance, R. Siragusa, P. Lemaître-Auger, and E. Perret, "Contactless characterization of coplanar stripline discontinuities by rcs measurement," *IEEE Trans. Antennas Propag.*, vol. 65, no. 1, pp. 251–257, 2016.

[26] E. Chen and S. Y. Chou, "Characteristics of coplanar transmission lines on multilayer substrates: Modeling and experiments," *IEEE Trans. Microw. Theory Tech.*, vol. 45, no. 6, pp. 939–945, 1997.

[27] T. K. Sarkar and O. Pereira, "Using the matrix pencil method to estimate the parameters of a sum of complex exponentials," *IEEE Antennas Propag. Mag.*, vol. 37, no. 1, pp. 48–55, 1995.

[28] Z. Ali, E. Perret, N. Barbot, and R. Siragusa, "Extraction of aspect-independent parameters using spectrogram method for chipless frequency-coded rfid," *IEEE Sensors J.*, vol. 21, no. 5, pp. 6530–6542, 2020.

[29] Goodfellow.com. (2019). [accessed 28 oct. 2019]. [Online]. Available: http://www.goodfellow.com/PDF/TAB004F.pdf

[30] L. Benkhaoua, M. T. Benhabiles, S. Mouissat, and M. L. Riabi, "Miniaturized quasi-lumped resonator for dielectric characterization of liquid mixtures," *IEEE Sensors J.*, vol. 16, no. 6, pp. 1603–1610, 2015.

[31] N. D. Orloff, J. Obrzut, C. J. Long, T. Lam, P. Kabos, D. R. Novotny, J. C. Booth, and J. A. Liddle, "Dielectric characterization by microwave cavity perturbation corrected for nonuniform fields," *IEEE Transactions on Microwave Theory and Techniques*, vol. 62, no. 9, pp. 2149–2159, 2014.

[32] M. Rahman, M. Islam, and M. Samsuzzaman, "Design and analysis of a resonator based metamaterial for sensor applications," *Microwave and Optical Technology Letters*, vol. 60, no. 3, pp. 694–698, 2018.

[33] M. Islam, M. Rahman, M. Mahmud, M. Ullah, M. Samsuzzaman, and M. Singh, "Investigation of a resonator-based metamaterial for sensor applications," *Applied Physics A*, vol. 124, pp. 1–7, 2018.

[34] A. Ebrahimi, J. Scott, and K. Ghorbani, "Differential sensors using microstrip lines loaded with two split-ring resonators," *IEEE Sensors J.*, vol. 18, no. 14, pp. 5786–5793, 2018.

[35] I. M. Rusni, A. Ismail, A. R. H. Alhawari, M. N. Hamidon, and N. A. Yusof, "An aligned-gap and centered-gap rectangular multiple split ring resonator for dielectric sensing applications," *Sensors*, vol. 14, no. 7, pp. 13 134–13 148, 2014.